

# Mixed phase of stannic and stannous oxide and their relation to crystallinity

N. Usharani<sup>1</sup>, R. P. Kumar<sup>2</sup>, A.S. Bhattacharyya<sup>3,4 a)</sup>, A. Raju<sup>1 b)</sup>

<sup>1</sup>Department of Physics & Electronics, Chaitanya - Deemed to be University,  
Hanamkonda, Telangana 506001 India.

<sup>2</sup>Department of Computer Science and Engineering. Nalla Malla Reddy Engineering College  
Divyanagar, Medchal, Hyderabad 500088

<sup>3</sup>Department of Metallurgical and Materials Engineering &

<sup>4</sup>Centre of Excellence in Green and Efficient Energy Technology (CoE GEET)  
Central University of Jharkhand, Brambe, Ranchi: 835205, India

Corresponding authors:

a) [2006asb@gmail.com](mailto:2006asb@gmail.com) (A.S. Bhattacharyya)

b) [amireddyraju123@gmail.com](mailto:amireddyraju123@gmail.com) (A. Raju)

## ABSTRACT

Stannic oxide, Sn (IV) O<sub>2</sub> synthesized by the sol-gel method showed heterogeneous crystallinity involving traces of stannous oxide, Sn (II) O as well which were studied based on the nucleation sites and aggregation of crystallites. The height to width ratio (HWR) was found to be an effective means of analyzing the growth process which involved lateral atomic diffusion and reversible phase transitions. The crystallinity and aggregation to larger crystallites is beneficial for electron transfer layer (ETL) in perovskite solar cells. The structure and morphology were determined by XRD and SEM-EDAX

**Keywords:** Stannic oxide, stannous oxide, electron transfer later, crystallinity, aggregation

## 1. INTRODUCTION

Following Min et al.'s research on tin (IV) oxide (Stannic Oxide, SnO<sub>2</sub>) as an efficient electron transport layer (ETL) in planar perovskite solar cells (PSC) as an alternative to previously employed TiO<sub>2</sub> [1], The field of research in the region continues to attract the interest of researchers, prompting them to make changes and improvements in order to improve output and power conversion efficiencies (PCE). The addition of SnO<sub>2</sub> resulted in a 25% gain in efficiency by giving stability to the n-i-p design. Interfacial flaws impede the charge transfer process, which is critical to the device's functionality. By producing a coherent interface, the metal oxide layer overcomes the problem. Because of high crystallinity or higher nucleation densities during synthesis, SnO<sub>2</sub> has high electron mobility as well as high optical transparency, which aids the above cause. [2-5]. However, there are a few obstacles in the usage of SnO<sub>2</sub> for PSC, such as hysteresis and crystallinity management. Although the addition of metals such as Aluminum (Al<sup>+3</sup>) and Nb<sub>2</sub>O<sub>5</sub>, as well as the usage of chemicals such as ammonium chloride and ethylene diamine tetra acetic acid (EDTA), has alleviated the problem to some extent, it may complicate the overall chemical composition and make technological intervention harder. [6-9]. This communication shows the formation of Tin oxides having dual oxidations states (+2 and + 4) and analyze the growing mechanism that affects ETL performance in PSC.

## 2. MATERIALS & METHODS

The SnO<sub>2</sub> was synthesized using the sol-gel technique which consisted of using tin (IV) tetrachloride (SnCl<sub>4</sub>. 2H<sub>2</sub>O) dissolved in ethanol (C<sub>2</sub>H<sub>5</sub> OH). Acetyl acetone (Ac Ac) was added dropwise for the hydrolysis of SnO<sub>2</sub>. Polyethylene glycol (PEG) was added as a binding agent. The sol was dried at 100 °C for 30 min followed by being crushed in a mortar pestle and calcined at 500 °C for 1 hour [10]. All the analytical grade reagents were received from Merck Pvt. Ltd without further purification. The characterizations were done using XRD (Proto A-XRD with Cu Kα source having 1.54 Å wavelength), FESEM (Zeiss, Germany) UV-Vis spectrometer (UV 3600 Plus, Shimadzu, Japan, and Photoluminescence spectrometer (Fluoromax-4, Horiba Scientific, USA). ImageJ software was used to obtain the linear and surface profiles.

## 3. RESULTS & DISCUSSIONS

The XRD pattern showed the formation of a phase close to the *cassiterite* tetragonal phase of tin dioxide (SnO<sub>2</sub>) having P<sub>42/mnm</sub> space group (JCPDS No. 41-1455) with dominant orientation along (110) and (101) planes (**Fig 1a**). There were evidences of formation of tetragonal SnO phase as well with cell parameters  $a = 3.80 \text{ \AA}$  and  $c = 4.84 \text{ \AA}$  which are in good agreement with (JCPDS, no. 06-0395). The weak reflections observed along (002) and (321) planes had mixed phase of Sn (II, IV) oxides. The crystallite size determined by FESEM showed variations (**Fig 2a**). The lowest size was around 20 nm which underwent clustering to form larger sizes as observed from the line profile with regions numbered 1 to 4 (**Fig 2b**). A region in SEM was taken for both surface profile and EDAX studies (**Fig 3a, b**). A high atomic percentage of oxygen (72.56%) was found to make SnO and SnO<sub>2</sub> with Sn being present in (27.44%). The surface profile was deconvoluted into different peaks with parameters given in **Table 1**. The width indicated the coagulation and height the nucleation intensity. The height to width ratio (HWR) can be considered as an indirect parameter to quantify the crystallization process.

**Table 1.** The fitting parameters for Fig 2(c)

Area	Centre	Width	Height	HWR
-53229.54005	110.57353	91.55301	-463.89549	voids
20378.24875	86.31395	64.07692	253.74954	3.97
24693.10083	130.74502	64.95228	303.33413	4.66
-15973.39622	275.00971	52.40277	-243.21091	void
-93.24147	262.51881	0.3056	-243.43856	void
2.28818E36	1.86764E28	4.38699E27	4.16164E8	42
13090.05887	274.3635	45.98686	227.11608	0.95
431.40391	339.78731	15.26871	22.54353	1.47
4.15232E76	1.33046E71	2.6482E70	1.25107E6	0.47
-3377.93931	365.68118	0.0019	-1.41942E6	void

The nucleation and growth of thin films involves the formation of crystal nuclei followed by evolution into the island, formation of network microstructure, and the growth of the networks into a continuous film [11, 12]. The whole process however starts with Gibb's free energy change of heterogeneous nucleation ( $\Delta G_{het}$ ) which is related to the HWR. The change in Gibbs free energy has two contributions, one from the surface ( $\Delta G_s$ ) which is related to the peak width as it indicates the amount of clustering and agglomeration that has taken place due to surface energy  $\gamma$ . The  $\Delta G_s$  is represented as  $4\pi r^2 \gamma$ . The other contribution comes from coalescence where the crystallites are merging together by atomic diffusion and involves release of energy due to reduction in area. They correspond to an increased value of HWR and phase transformation. The plot of HWR with crystallite size showed a sudden decrease in slope. The crystallite size corresponding to the change is the critical radius ( $r^* = 30 \text{ nm}$ ). For crystallite size greater than  $r^*$ , clustering is dominant forming larger crystallites. The slope of the plot for  $r < r^* = 0.02$  and  $r > r^* = 0.01$ . A lower HWR is desirable as clustering causes higher power conversion efficiencies (PCE) with negligible hysteresis providing stability to the device [6]. The HWR corresponding to  $r^*$  was 2.5 (**Fig 2c**). The HWR of the surface as again found symmetrically distributed surrounding that value (**Fig 3d**) at  $7 \mu\text{m}$  for the total scan length of  $14 \mu\text{m}$ . The HWR attain saturation in both upper and lower values. The larger crystallites are associated with larger Gibbs free energy change; The aggregation of atoms to form islands is dependent on the surface diffusion and nucleation rate which is inversely proportional to HWR. The Gibbs free energy for SnO<sub>2</sub> formation is  $51.82 \text{ J/mol K}$  which is more stable than SnO. An increase in particle size due to aggregation therefore depicts higher amounts of SnO<sub>2</sub> formation. SnO<sub>2</sub> being an electron transfer layer, its efficiency gets enhanced due to aggregation of crystallites which involved atomic diffusion and phase transformation involving reversible phase transitions between the dual valency of Sn (+2 and +4). The presence of Sn in lower oxidation states forming SnO providing p-type conductivity has also served in enhancing the efficiency of the ETL. These two phenomena shows that although formation of larger crystallites of the stable phase of SnO<sub>2</sub> is beneficial for the ETL, the smaller SnO crystallites involved in the aggregation process may further add to the cause. The aggregation process after forming a crystallites  $2.3 \mu\text{m}$  can be seen to take two different paths, the one which has higher rate of formation ( $\Delta G$ ) indicates a lower percentage of SnO (process 1). The other process, involving a lower rate (process 2) is more likely

to have a higher percentage of SnO which shall cause a higher ETL ability (Fig 3e). The average crystallite size was 18 nm as obtained from particle size analysis. (Fig 3f).

#### 4. CONCLUSIONS

Stannic and stannous oxide crystallites prepared by sol-gel showed heterogeneous crystallinity. The height to width ratio (HWR) in the crystallization morphology was used in understanding the growth process involved. The results indicate the significance of the crystallinity and aggregation in the electron transport phenomenon in SnO<sub>2</sub> making them applicable as an ETL in perovskite solar cells. The crystalline morphology was studied by means of height to width ratio (HWR). The presence of reversible dual oxidation states of Sn (+2 and +4) helps in enhancing the

electron transport layer property of SnOx. The crystallite aggregation process after a certain progress can perform even better as an ETL if a reversible transition involving formation of SnO takes place.

#### DECLARATIONS

Compliance with Ethical Standards

The manuscript has not been submitted in parallel either in full or partially to any other journal.

Conflict of interest

There is no conflict of interest among the authors

Research Data Policy and Data Availability Statements

Data shall be provided on request

#### FUNDING

No funding was received for conducting the research

#### REFERENCE

1. H. Min et al Nature (2021) 598, 444-450.
2. H. Fang RRL Solar (2020), 4, 1900425.
3. S.Y. Park, K. Zhu Adv Mat (2022) 37, 2110438.
4. X. Huang et al RRL Solar (2020) 43, 1900336.
5. J. Li et al Chemsus Chem (2018) 11, 2898-2903
6. Z. Liu et al Angewandte Chem (2019) 58, 11497 – 11504
7. R. Litze et al Adv Mat (2000) 12, 165-168.
8. D. Yang et al Nat Comm (2018) 9, 3239.
9. H. Chen et al Nanoscale Res Lett (2017) 12, 1-6.
10. M Aziz et al Materials Letters (2013) 91, 31–34.
11. A. Zhumekenov et al ACS Energy Lett (2017) 2, 1782 – 1788.
12. H. Zhao et al J. Mater Chem A (2018) 6, 10825- 10834.
13. J. Euvrad et al Mater. Adv., **2021,2, 2956-2965**
14. A. R. Zanatta, Scientific Reports (2019) 9, 11225.
15. A Doyan et al 2021 J. Phys.: Conf. Ser. **1816 012114**
16. P.S. Shewale et al J. Lumin (2013) 139, 113-118.
17. C. Chen et al AL J Mater Sci: Mater Electron (2017) 28, 18603–18609

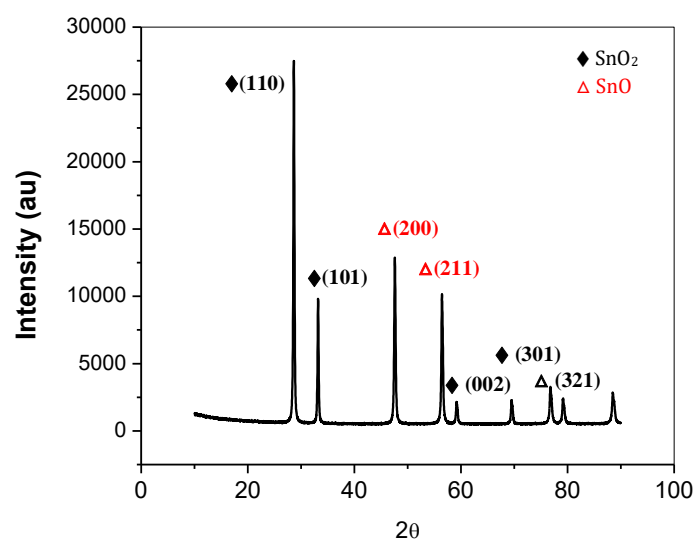


Fig 1 XRD showing a mixed phase of  $\text{SnO}_2$  and  $\text{SnO}$

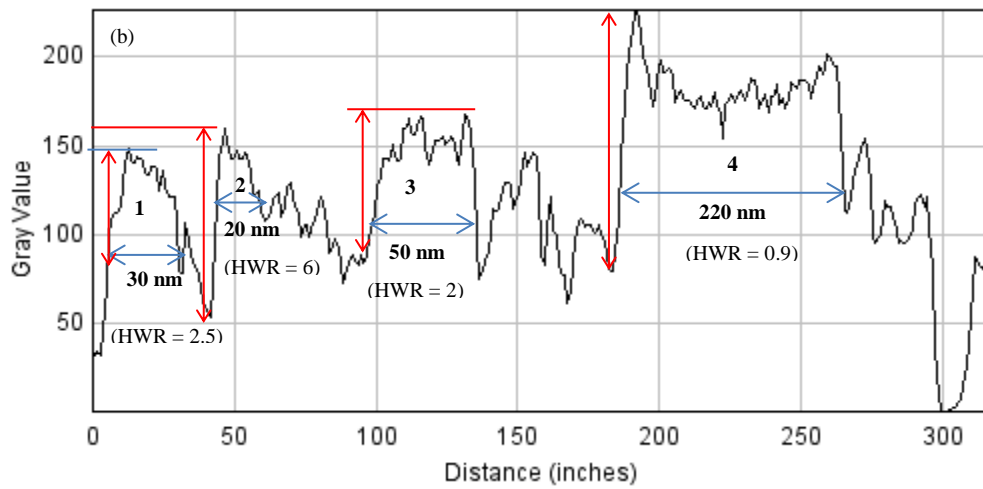
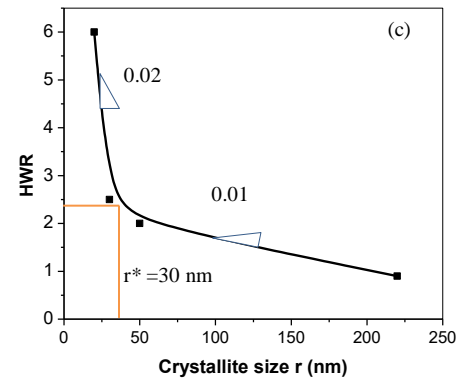
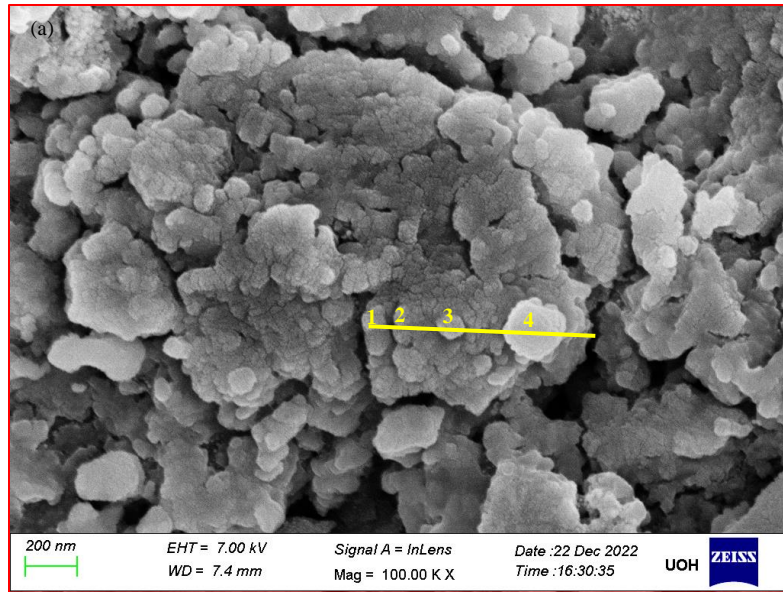
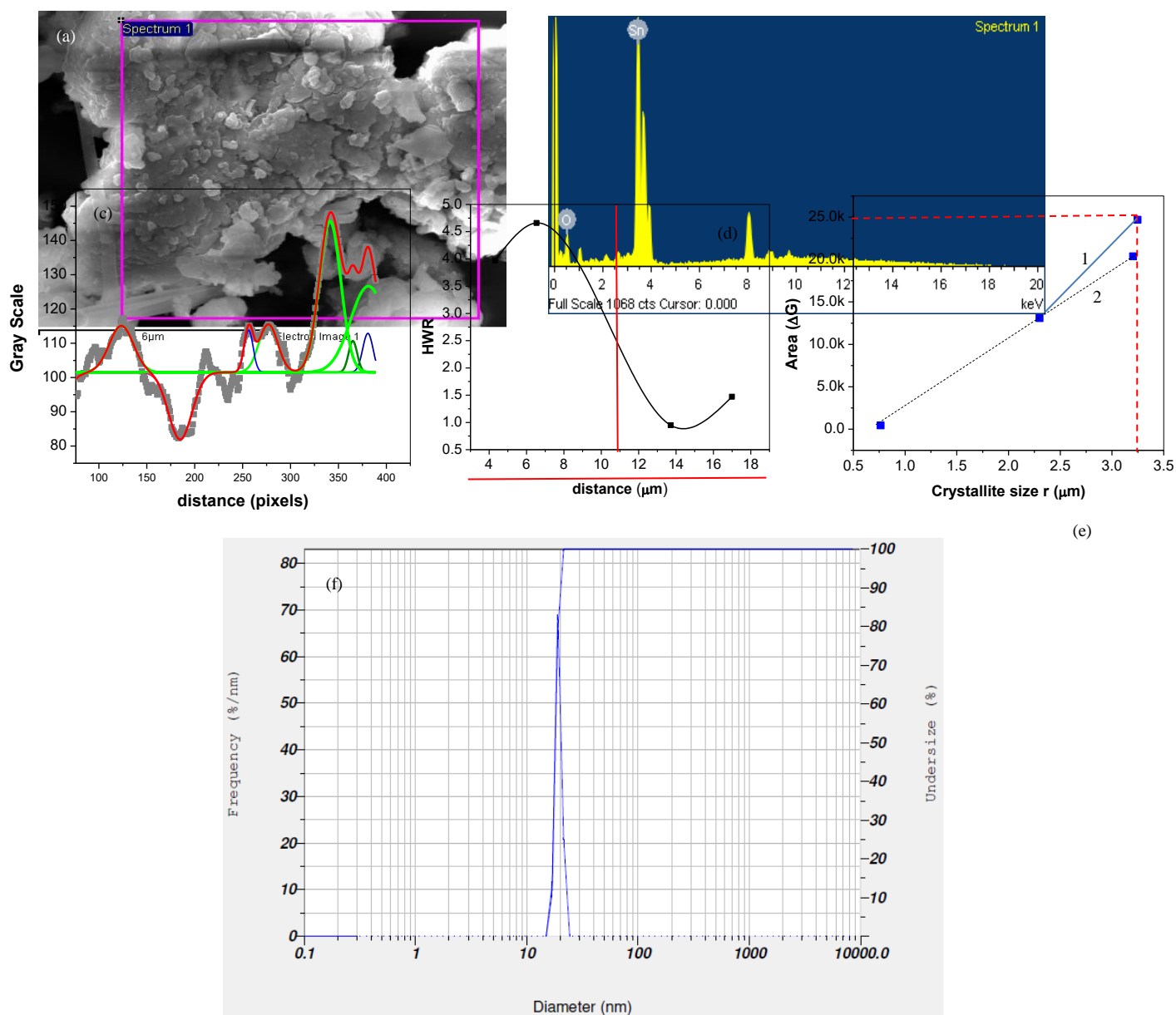


Fig 2: (a) FESEM of Stannic Oxide showing the formation of nano crystallites with (b) linear profile giving the HWR values of 4 crystallites as marked in the image



**Fig 3.** The SEM image and (b) EDAX spectra showing the elemental composition (c) surface profile of the same region of the synthesized Stannic Oxide (d) The variation of HWR with scan distance (e) The dual aggregation process (f) particle size analyzer showing average size of 18 nm.